

Hybrid Trilinear and Bilinear Programming for Aligning Partially Overlapping Point Sets

Wei Lian, Wangmeng Zuo and Lei Zhang

Abstract—Alignment methods which can handle partially overlapping point sets and are invariant to the corresponding transformations are desirable in computer vision, with applications such as providing initial transformation configuration for local search based methods like ICP. To this end, we first show that the objective of the robust point matching (RPM) algorithm is a cubic polynomial. We then utilize the convex envelopes of trilinear and bilinear monomials to develop its lower bounding function. The resulting lower bounding problem can be efficiently solved via linear assignment and low dimensional convex quadratic programming. We next develop a branch-and-bound (BnB) algorithm which only branches over the transformation parameters and converges quickly. Experimental results demonstrated favorable performance of the proposed method over the state-of-the-art methods in terms of robustness and speed.

Index Terms—branch and bound, concave optimization, linear assignment, point correspondence, robust point matching

I. INTRODUCTION

Point matching is a fundamental problem in computer vision and pattern recognition. Disturbances such as deformation, occlusion, outliers and unknown poses make this problem very challenging. One way of achieving point matching is through optimization of the objective of the RPM algorithm [6]. By eliminating the transformation variable, [16] reduces the objective to a concave quadratic function of point correspondence with a low rank Hessian matrix. It then employs the normal rectangular algorithm, a variant of the BnB algorithm, for optimization. But the method requires that one point set can be embedded in another set.

To relax this requirement, [14] reduces the objective of RPM to a concave function of point correspondence, which, albeit not quadratic, still has a low rank structure. It then employs the normal simplex algorithm, a variant of the BnB algorithm, for optimization. But the BnB algorithm branches over a projected space of point correspondence, whose dimension is quite larger than the number of transformation parameters, causing the method to converge slowly. On the other hand, the BnB algorithm requires that the objective function is concave over a sufficiently large region, whereas it is only concave over

a finite region. To address this issue, the method enlarges the concavity region of the objective function by using regularization on transformation, where prior information about the values of transformation parameters needs to be supplied. But this causes the method biased towards yielding transformation solutions only consistent with the prior information.

To address this issue, [15] utilizes the constraints of 2D/3D rigid transformations to develop a new objective function of point correspondence which is always concave. Thus, no regularization on transformation is needed and the method is invariant to the corresponding transformation. But like [14], the BnB algorithm still branches over a projected space of point correspondence, causing the method to converge slowly.

In this paper, we propose an alternative BnB based approach to optimize the objective of RPM. We argue that it is advantageous to keep the transformation variable instead of eliminating them as are the practice in [16], [14], [15]. First, we show that the objective of RPM is a cubic polynomial. Then, we utilize the convex envelopes of trilinear and bilinear monomials to develop a lower bounding function of the objective of RPM. The resulting lower bounding problem can be efficiently solved via linear assignment and low dimensional convex quadratic programming. Next, we show that for the lower bounding function to converge to the objective function, we only need to branch over the transformation variable. Thus, our method can converge much faster than those of [14], [15]. Finally, unlike [14], our method imposes no requirement on transformation, thus, it is invariant to the corresponding transformation.

The remainder of the paper is arranged as follows: In Sec. II, we review related work. In Sec. III, we present theoretical framework needed for the development of our lower bounding functions. In Sec. IV and V, we discuss our objective functions and optimization strategies under two different types of transformations. In Sec. VI, we present the BnB algorithm. In Sec. VII, we present experimental results.

II. RELATED WORK

A. Heuristic based methods

The methods related to ours are those modeling transformation and point correspondence. ICP [2], [24] iterates between estimating point correspondence and updating transformation. But it is prone to be trapped in local minima due to discrete nature of point correspondence. RPM [6] relaxes point correspondence to be soft valued and uses deterministic annealing (DA) for optimization. But DA is biased towards matching the mass centers of two point sets.

W. Lian is with the Department of Computer Science, Changzhi University, Changzhi, 046011, Shanxi, China, and the Department of Computing, The Hong Kong Polytechnic University, Hong Kong. E-mail: lianwei3@gmail.com.

W.-M. Zuo is with School of Computer Science and Technology, Harbin Institute of Technology (HIT), Harbin, China. E-mail: cswmzuo@gmail.com.

L. Zhang is with the Department of Computing, The Hong Kong Polytechnic University, Hung Hom, Kowloon, Hong Kong. E-mail: cszlzhang@comp.polyu.edu.hk.

The second category of methods are those modeling only transformation. The CPD method [20] casts point matching as the problem of fitting a Gaussian Mixture Model (GMM) representing one point set to another point set. The GMMREG method [12] uses GMMs to represent two point sets and minimizes the L_2 -norm distance between them. Support vector parameterized Gaussian mixtures (SVGMS) has been proposed in [3] to represent point sets using sparse Gaussian components. The efficiency of GMM based methods is improved by using filtering to solve the correspondence problem in [8].

B. Global optimization based methods

The BnB algorithm is a popular global optimization technique. It is used to align 3D shapes based on the Lipschitz optimization theory [13]. But the method assumes no occlusion or outliers. BnB is used to recover 3D rigid transformation in [21]. But the correspondence needs to be known a priori. The Go-ICP method [11] uses BnB to optimize the ICP objective by exploiting the structure of the geometry of 3D rigid motions. The GOGMA method registers two point sets by aligning the GMMs constructed from the original point sets [4]. The fast rotation search (FRS) method [1], [22] recovers 3D rotation by using stereographic projection. Rigid registration is achieved via a nested BnB algorithm. A rotation-invariant feature is proposed in [17], leading to a more efficient BnB based algorithm. Bayesian nonparametric point set representation and a new way of tessellating rotation space are proposed in [23].

III. CONVEX ENVELOPE LINEARIZATION

A. Bilinear monomial

The convex envelope of a bilinear monomial xy , $\underline{x} \leq x \leq \bar{x}$, $\underline{y} \leq y \leq \bar{y}$ is well known to be

$$(xy)_{l1} \triangleq \underline{xy} + \underline{xy} - \underline{xy} \leq xy \quad (1)$$

$$(xy)_{l2} \triangleq \bar{xy} + \bar{xy} - \bar{xy} \leq xy \quad (2)$$

If we adopt this form of convex envelope when designing the lower bounding function of our objective function, either the form of $\max\{(xy)_{l1}, (xy)_{l1}\}$ needs to be incorporated into the lower bounding function or subproblem in the form of $\min\{\alpha|\alpha \geq (xy)_{l1}, \alpha \geq (xy)_{l1}\}$ needs to be incorporated into the lower bounding problem. For the former case, the lower bounding function is convex but not linear, thus requiring multiple steps of optimization, which is slow and susceptible to numerical inaccuracy issues. For the latter case, the lower bounding problem may not take the form of a combinatorial optimization problem. Consequently, no combinatorial optimization algorithms can be employed and our algorithm will be inefficient.

To address the above issues, we instead construct a new linear lower bounding function $(xy)_l$ of xy by averaging the above inequalities:

$$(xy)_l \triangleq \frac{1}{2} \sum_i (xy)_{li} \leq xy \quad (3)$$

We note that similar idea has been employed in [9] for upper bound linearization.

[5] shows that for a bilinear monomial, for its convex envelope to converge to it, we only need to branch over one variable that makes up the bilinear monomial. Similar conclusion can also be drawn about our linear lower bounding function (3). The proof is presented in the Appendix.

B. Trilinear monomial

The convex envelope of a trilinear monomial $x_i x_j x_k$ depends on the signs of the bounds on variables [18], [19]. Denoting a permutation of x_i, x_j, x_k by the symbols x, y, z , where $\underline{x} \leq x \leq \bar{x}$, $\underline{y} \leq y \leq \bar{y}$ and $\underline{z} \leq z \leq \bar{z}$, in the case $\underline{x} \leq 0, \underline{y} \geq 0, \underline{z} \leq 0, \bar{z} \geq 0$, we can get the following convex envelope:

$$(xyz)_{l1} \triangleq \underline{y}\bar{z}x + \bar{x}\bar{z}y + \bar{x}\bar{y}z - 2\bar{x}\bar{y}\bar{z} \leq xyz \quad (4)$$

$$(xyz)_{l2} \triangleq \underline{y}\bar{z}x + \underline{x}\bar{z}y + \underline{x}\bar{y}z - \underline{x}\bar{y}\bar{z} - \underline{x}\bar{y}\bar{z} \leq xyz \quad (5)$$

$$(xyz)_{l3} \triangleq \underline{y}\bar{z}x + \underline{x}\bar{z}y + \underline{x}\bar{y}z - \underline{x}\bar{y}\bar{z} - \underline{x}\bar{y}\bar{z} \leq xyz \quad (6)$$

$$(xyz)_{l4} \triangleq \underline{y}\bar{z}x + \bar{x}\bar{z}y + \bar{x}\bar{y}z - \bar{x}\bar{y}\bar{z} - \bar{x}\bar{y}\bar{z} \leq xyz \quad (7)$$

$$(xyz)_{l5} \triangleq \underline{y}\bar{z}x + \bar{x}\bar{z}y + \underline{x}\bar{y}z - \bar{x}\bar{y}\bar{z} - \underline{x}\bar{y}\bar{z} \leq xyz \quad (8)$$

$$(xyz)_{l6} \triangleq \underline{y}\bar{z}x + \underline{x}\bar{z}y + \phi/(\bar{z} - \underline{z})z - \phi\underline{z}/(\bar{z} - \underline{z}) - \underline{x}\bar{y}\bar{z} - \bar{x}\bar{y}\bar{z} + \bar{x}\bar{y}\bar{z} \leq xyz \quad (9)$$

where $\phi = \underline{x}\bar{y}\bar{z} - \bar{x}\bar{y}\bar{z} - \underline{x}\bar{y}\bar{z} + \bar{x}\bar{y}\bar{z}$.

Based on the same consideration as stated in Sec. III-A, we do not directly utilize this form of lower convex envelope. Instead, we construct a new linear lower bounding function $(xyz)_l$ of xyz by averaging the above inequalities:

$$(xyz)_l \triangleq \frac{1}{6} \sum_i (xyz)_{li} \leq xyz \quad (10)$$

For other cases of the bounds on x, y, z , we conduct similar operations to linearize the corresponding convex envelopes.

In a similar vein as in Sec. III-A, for a trilinear monomial, for its linear lower bounding function to converge to it, we only need to branch over two variables that make up the trilinear monomial. The proof is presented in the Appendix.

IV. CASE ONE: TRANSFORMATION IS LINEAR W.R.T. ITS PARAMETERS

Suppose there are two point sets $\mathcal{X} = \{\mathbf{x}_i, 1 \leq i \leq n_x\}$ and $\mathcal{Y} = \{\mathbf{y}_j, 1 \leq j \leq n_y\}$ in \mathbb{R}^{n_d} to be aligned, where \mathbf{x}_i and \mathbf{y}_j are column vectors. To solve this problem, following [14], we model point set alignment as a mixed linear assignment–least square problem:

$$\begin{aligned} \min E(\mathbf{P}, \boldsymbol{\theta}) &= \sum_{i,j} p_{ij} \|\mathbf{y}_j - \mathbf{J}(\mathbf{x}_i)\boldsymbol{\theta}\|^2 = \mathbf{1}_{n_x}^\top \mathbf{P} \tilde{\mathbf{y}} \\ &+ \boldsymbol{\theta}^\top \mathbf{J}^\top (\text{diag}(\mathbf{P}\mathbf{1}_{n_y}) \otimes \mathbf{I}_d) \mathbf{J} \boldsymbol{\theta} - 2\boldsymbol{\theta}^\top \mathbf{J}^\top (\mathbf{P} \otimes \mathbf{I}_d) \mathbf{y} \quad (11) \\ \text{s.t. } &\mathbf{P}\mathbf{1}_{n_y} \leq \mathbf{1}_{n_x}, \mathbf{1}_{n_x}^\top \mathbf{P} \leq \mathbf{1}_{n_y}^\top, \mathbf{1}_{n_x}^\top \mathbf{P} \mathbf{1}_{n_y} = n_p, \\ &\mathbf{P} \geq 0, \boldsymbol{\theta}_0 \leq \boldsymbol{\theta} \leq \bar{\boldsymbol{\theta}}_0 \quad (12) \end{aligned}$$

where the spatial transformation $T(\mathbf{x}_i|\boldsymbol{\theta}) = \mathbf{J}(\mathbf{x}_i)\boldsymbol{\theta}$ is chosen to be linear w.r.t. its parameters $\boldsymbol{\theta}$, where $\mathbf{J}(\mathbf{x}_i)$ is called the Jacobian matrix. \mathbf{P} denotes a correspondence matrix with element $p_{ij} = 1$ indicating that there is a matching between \mathbf{x}_i and \mathbf{y}_j and $p_{ij} = 0$ otherwise. The constraint

$\mathbf{1}_{n_x}^\top \mathbf{P} \mathbf{1}_{n_y} = n_p$ indicates that the number of matches is required to be equal to n_p , a predefined positive integer. The matrix $\mathbf{J} \triangleq [\mathbf{J}^\top(\mathbf{x}_1), \dots, \mathbf{J}^\top(\mathbf{x}_{n_x})]^\top$ and the vectors $\mathbf{y} \triangleq [\mathbf{y}_1^\top, \dots, \mathbf{y}_{n_y}^\top]^\top$, $\tilde{\mathbf{y}} \triangleq [\|\mathbf{y}_1\|_2^2, \dots, \|\mathbf{y}_{n_y}\|_2^2]^\top$. $\mathbf{1}_{n_x}$ denotes the n_x -dimensional vector of all ones. \mathbf{I}_d denotes the $d \times d$ identity matrix. $\text{diag}(\cdot)$ converts a vector into a diagonal matrix. \otimes denotes the Kronecker product. The constant vectors $\underline{\theta}_0$ and $\bar{\theta}_0$ define the bounds of θ .

To facilitate optimization of E , \mathbf{P} needs to be vectorized. We define the vectorization of a matrix as the concatenation of its rows, denoted by $\text{vec}(\cdot)$. Let $\mathbf{p} \triangleq \text{vec}(\mathbf{P})$. To obtain a concise form of E , we will introduce new denotations. Let

$$\mathbf{1}_{n_x}^\top \tilde{\mathbf{P}} \mathbf{y} = \rho^\top \mathbf{p}, \quad \mathbf{J}^\top (\mathbf{P} \otimes \mathbf{I}_{n_d}) \mathbf{y} = \mathbf{A} \mathbf{p}, \quad (13)$$

$$\begin{aligned} \text{vec}(\mathbf{J}^\top (\text{diag}(\mathbf{P} \mathbf{1}_{n_y}) \otimes \mathbf{I}_{n_d}) \mathbf{J}) = \\ \text{vec}(\mathbf{J}_2^\top ((\mathbf{P} \mathbf{1}_{n_y}) \otimes \mathbf{I}_{n_\theta})) = \mathbf{B} \mathbf{p} \end{aligned} \quad (14)$$

where n_θ denotes the dimension of θ and matrix $\mathbf{J}_2 \triangleq [\mathbf{J}^\top(\mathbf{x}_1)^\top \mathbf{J}(\mathbf{x}_1), \dots, \mathbf{J}^\top(\mathbf{x}_{n_x})^\top \mathbf{J}(\mathbf{x}_{n_x})]^\top$. Based on the fact that $\text{vec}(\mathbf{M}_1 \mathbf{M}_2 \mathbf{M}_3) = (\mathbf{M}_1 \otimes \mathbf{M}_3^\top) \text{vec}(\mathbf{M}_2)$ for any multiplicable matrices \mathbf{M}_1 , \mathbf{M}_2 and \mathbf{M}_3 , we get the results that

$$\rho = \mathbf{1}_{n_x} \otimes \tilde{\mathbf{y}}, \quad \mathbf{A} = (\mathbf{J}^\top \otimes \mathbf{y}^\top) \mathbf{W}_{n_d}^{n_x, n_y}, \quad (15)$$

$$\mathbf{B} = (\mathbf{J}_2^\top \otimes \mathbf{I}_{n_\theta}) \mathbf{W}_{n_\theta}^{n_x, 1} (\mathbf{I}_{n_x} \otimes \mathbf{1}_{n_y}^\top) \quad (16)$$

where the $mnd^2 \times mn$ constant matrix $\mathbf{W}_d^{m, n} \triangleq \mathbf{I}_m \otimes [\mathbf{I}_n \otimes (\mathbf{e}_d^1)^\top, \dots, \mathbf{I}_n \otimes (\mathbf{e}_d^d)^\top]^\top$ satisfies $\text{vec}(\mathbf{C}_{m, n} \otimes \mathbf{I}_d) = \mathbf{W}_d^{m, n} \text{vec}(\mathbf{C}_{m, n})$ [14]. Here \mathbf{e}_d^i denotes the d -dimensional column vector with the i -th entry being 1 and all other entries being 0. $\mathbf{W}_d^{m, n}$ is a large but sparse matrix and can be implemented using the function *speye* in Matlab.

With the above preparation, E can be rewritten as:

$$E(\mathbf{p}, \theta) = \theta^\top \text{mat}(\mathbf{B} \mathbf{p}) \theta - 2\theta^\top \mathbf{A} \mathbf{p} + \rho^\top \mathbf{p} \quad (17)$$

where $\text{mat}(\cdot)$ denotes reconstructing a matrix from a vector, which can be viewed as the inverse of the operator $\text{vec}(\cdot)$.

Since $\mathbf{1}_{n_x n_y}^\top \mathbf{p} = n_p$, a constant, for rows of \mathbf{B} containing identical elements, the result of them multiplied by \mathbf{p} can be replaced by constants. Also, redundant rows can be removed. Since $\text{mat}(\mathbf{B} \mathbf{p})$ is a symmetric matrix, \mathbf{B} will contain redundant rows. Based on these analyses, we hereby denote \mathbf{B}_2 as the matrix formed as a result of \mathbf{B} removing such rows. (Please refer to Sec. VII-A for examples of \mathbf{B}_2). Consequently, E can be rewritten as

$$E(\mathbf{p}, \theta) = \theta^\top [\text{mat}(\mathbf{K} \mathbf{B}_2 \mathbf{p}) + \mathbf{C}] \theta - 2\theta^\top \mathbf{A} \mathbf{p} + \rho^\top \mathbf{p} \quad (18)$$

where the nonzero elements of the constant matrix \mathbf{C} correspond to the rows of \mathbf{B} containing identical elements. The elements of the constant matrix \mathbf{K} take values in $\{0, 1\}$ and record the correspondences between the rows of \mathbf{B}_2 and those of \mathbf{B} .

In the following, first, we reformulate the objective function due to a requirement when using the convex envelope of a trilinear monomial [19] (Sec. IV-A). Then, we discuss the branching strategy (Sec. IV-B). Next, we derive the lower bounding functions of bilinear and trilinear terms (Sec. IV-C and IV-D). These results are used to build the lower bounding function of the objective function (Sec. IV-E). Finally, we discuss the computation of upper bound (Sec. IV-F).

A. Objective function reformulation

[19] only presents the convex envelope of a trilinear monomial under the condition that at least one variable that makes up the monomial has a range containing the origin, whereas for the trilinear term $\theta^\top \text{mat}(\mathbf{K} \mathbf{B}_2 \mathbf{p}) \theta$ in our objective function, such a condition can be violated. To address this issue, since our branching strategy (to be presented in Sec. IV-B) is that the range of θ_i changes during the BnB iterations, whereas the range of $[\text{mat}(\mathbf{K} \mathbf{B}_2 \mathbf{p})]_{ij}$ remains fixed, therefore, we seek to replace $\text{mat}(\mathbf{K} \mathbf{B}_2 \mathbf{p})$ by a proper matrix such that this condition can be satisfied. The procedure is as follows:

We build a constant symmetric matrix \mathbf{D} such that all the elements of $\text{mat}(\mathbf{K} \mathbf{B}_2 \mathbf{p}) - \mathbf{D}$ have ranges containing the origin. This can be accomplished as follows: We first choose $\mathbf{p}_0 \in \Omega$, where Ω denotes the feasible region of \mathbf{p} , as is defined by (12). (In this paper, \mathbf{p}_0 is chosen as $\frac{n_p}{n_x n_y} \mathbf{1}_{n_x n_y}$, corresponding to the fuzziest point correspondence.) We then let $\mathbf{D} = \text{mat}(\mathbf{K} \mathbf{B}_2 \mathbf{p}_0)$. We now have

Proposition 1: All the elements of $\text{mat}(\mathbf{K} \mathbf{B}_2 \mathbf{p}) - \mathbf{D}$ have ranges containing the origin.

Proof Since $\mathbf{p}_0 \in \Omega$, we have $\mathbf{D} \in \{\text{mat}(\mathbf{K} \mathbf{B}_2 \mathbf{p}) | \mathbf{p} \in \Omega\}$. Therefore, $0 \in \{[\text{mat}(\mathbf{K} \mathbf{B}_2 \mathbf{p}) - \mathbf{D}]_{ij} | \mathbf{p} \in \Omega\}$.

Our experiments indicate that different choices of \mathbf{p}_0 (and thus \mathbf{D}) lead to almost the same alignment results. Based on the above analysis, E is reformulated as:

$$\begin{aligned} E(\mathbf{p}, \theta) = \theta^\top [\text{mat}(\mathbf{K} \mathbf{B}_2 \mathbf{p}) - \mathbf{D}] \theta + \theta^\top (\mathbf{C} + \mathbf{D}) \theta \\ - 2\theta^\top \mathbf{A} \mathbf{p} + \rho^\top \mathbf{p} \end{aligned} \quad (19)$$

B. Branching strategy

Based on the result in Sec. III-A, for the bilinear term $-2\theta^\top \mathbf{A} \mathbf{p}$, for its linear lower bounding function to converge to it, we only need to branch the range of θ and let the range of $-2\mathbf{A} \mathbf{p}$ fixed. Here the range of $-2\mathbf{A} \mathbf{p}$ is computed as $\min_{\mathbf{p} \in \Omega} (-2\mathbf{A} \mathbf{p})_i \leq (-2\mathbf{A} \mathbf{p})_i \leq \max_{\mathbf{p} \in \Omega} (-2\mathbf{A} \mathbf{p})_i$ via solving linear assignment problems.

In a similar vein, based on the result in Sec. III-B, for the trilinear term $\theta^\top [\text{mat}(\mathbf{K} \mathbf{B}_2 \mathbf{p}) - \mathbf{D}] \theta$, for its linear lower bounding function to converge to it, we only need to branch the range of θ and let the range of $\text{mat}(\mathbf{K} \mathbf{B}_2 \mathbf{p}) - \mathbf{D}$ fixed since θ constitutes two sets of variables that make up $\theta^\top [\text{mat}(\mathbf{K} \mathbf{B}_2 \mathbf{p}) - \mathbf{D}] \theta$. Here the range of $\text{mat}(\mathbf{K} \mathbf{B}_2 \mathbf{p}) - \mathbf{D}$ is computed as $\min_{\mathbf{p} \in \Omega} [\text{mat}(\mathbf{K} \mathbf{B}_2 \mathbf{p}) - \mathbf{D}]_{ij} \leq [\text{mat}(\mathbf{K} \mathbf{B}_2 \mathbf{p}) - \mathbf{D}]_{ij} \leq \max_{\mathbf{p} \in \Omega} [\text{mat}(\mathbf{K} \mathbf{B}_2 \mathbf{p}) - \mathbf{D}]_{ij}$ via solving linear assignment problems.

To sum up, in our BnB algorithm, we only need to branch over θ . Thus, the dimension of the branching space of our BnB algorithm is low and our algorithm can converge quickly.

C. Lower bounding function of the bilinear term

Based on the result in Sec. III-A, we can get the lower bounding function of $-2\theta^\top \mathbf{A} \mathbf{p}$ within ranges $\underline{\theta}_i \leq \theta_i \leq \bar{\theta}_i$ and $\min_{\mathbf{p} \in \Omega} (-2\mathbf{A} \mathbf{p})_i \leq (-2\mathbf{A} \mathbf{p})_i \leq \max_{\mathbf{p} \in \Omega} (-2\mathbf{A} \mathbf{p})_i$ by first computing the lower bounding functions of the individual terms $\theta_i (-2\mathbf{A} \mathbf{p})_i$:

$$g_i^0 \theta_i + g_i^1 (-2\mathbf{A} \mathbf{p})_i + g_i^2 \leq \theta_i (-2\mathbf{A} \mathbf{p})_i \quad (20)$$

where the constant vectors \mathbf{g}^k are computed based on the ranges of θ_i and $(-2\mathbf{A}\mathbf{p})_i$. Now, we can get the lower bounding function of $-2\boldsymbol{\theta}^\top \mathbf{A}\mathbf{p}$ by summing the above result over i :

$$\boldsymbol{\theta}^\top \mathbf{g}^0 + (\mathbf{g}^1)^\top (-2\mathbf{A}\mathbf{p}) + \mathbf{1}_{n_\theta}^\top \mathbf{g}^2 \leq -2\boldsymbol{\theta}^\top \mathbf{A}\mathbf{p} \quad (21)$$

D. Lower bounding function of the trilinear term

Based on the result in Sec. III-B, We can get the lower bounding function of $\boldsymbol{\theta}^\top [\text{mat}(\mathbf{K}\mathbf{B}_2\mathbf{p}) - \mathbf{D}]\boldsymbol{\theta}$ within ranges $\underline{\theta}_i \leq \theta_i \leq \bar{\theta}_i$ and $\min_{\mathbf{p} \in \Omega} [\text{mat}(\mathbf{K}\mathbf{B}_2\mathbf{p}) - \mathbf{D}]_{ij} \leq [\text{mat}(\mathbf{K}\mathbf{B}_2\mathbf{p}) - \mathbf{D}]_{ij} \leq \max_{\mathbf{p} \in \Omega} [\text{mat}(\mathbf{K}\mathbf{B}_2\mathbf{p}) - \mathbf{D}]_{ij}$ by first computing the lower bounding functions of the individual terms $\theta_i [\text{mat}(\mathbf{K}\mathbf{B}_2\mathbf{p}) - \mathbf{D}]_{ij} \theta_j$:

$$\begin{aligned} \theta_i H_{ij}^0 + [\text{mat}(\mathbf{K}\mathbf{B}_2\mathbf{p}) - \mathbf{D}]_{ij} H_{ij}^1 + H_{ij}^2 \\ \leq \theta_i [\text{mat}(\mathbf{K}\mathbf{B}_2\mathbf{p})]_{ij} \theta_j \end{aligned} \quad (22)$$

where the constant matrices \mathbf{H}^k are computed based on the ranges of θ_i and $[\text{mat}(\mathbf{K}\mathbf{B}_2\mathbf{p}) - \mathbf{D}]_{ij}$. Now, we can get the lower bounding function of $\boldsymbol{\theta}^\top [\text{mat}(\mathbf{K}\mathbf{B}_2\mathbf{p}) - \mathbf{D}]\boldsymbol{\theta}$ by summing the above result over i and j :

$$\begin{aligned} \boldsymbol{\theta}^\top \mathbf{H}^0 \mathbf{1}_{n_\theta} + \text{tr}([\text{mat}(\mathbf{K}\mathbf{B}_2\mathbf{p}) - \mathbf{D}]^\top \mathbf{H}^1) + \mathbf{1}_{n_\theta}^\top \mathbf{H}^2 \mathbf{1}_{n_\theta} \\ \leq \boldsymbol{\theta}^\top \text{mat}(\mathbf{K}\mathbf{B}_2\mathbf{p}) \boldsymbol{\theta} \end{aligned} \quad (23)$$

Here, $\text{tr}(\cdot)$ denotes the trace of a square matrix.

E. Lower bound of the objective function

Combining the results in Sec. IV-C and IV-D, we get lower bounding problem of the original problem (11), (12) as

$$\min E_l(\mathbf{p}, \boldsymbol{\theta}) \triangleq \boldsymbol{\theta}^\top (\mathbf{C} + \mathbf{D})\boldsymbol{\theta} + \mathbf{m}_0^\top \boldsymbol{\theta} + \mathbf{m}_1^\top \mathbf{p} + m_2 \quad (24)$$

$$\text{s.t. } \underline{\boldsymbol{\theta}} \leq \boldsymbol{\theta} \leq \bar{\boldsymbol{\theta}}, \mathbf{p} \in \Omega \quad (25)$$

where the constant vectors $\mathbf{m}_0 \triangleq \mathbf{H}^0 \mathbf{1}_{n_\theta} + \mathbf{g}^0$ and $\mathbf{m}_1 \triangleq \mathbf{B}_2^\top \mathbf{K}^\top \text{vec}(\mathbf{H}^1) - 2\mathbf{A}^\top \mathbf{g}^1 + \boldsymbol{\rho}$. The constant scalar $m_2 \triangleq \mathbf{1}_{n_\theta}^\top \mathbf{g}^2 - \text{tr}(\mathbf{D}^\top \mathbf{H}^1) + \mathbf{1}_{n_\theta}^\top \mathbf{H}^2 \mathbf{1}_{n_\theta}$.

It is obvious that this problem can be decomposed into separate optimizations over \mathbf{p} and $\boldsymbol{\theta}$. \mathbf{p} can be recovered by solving the following linear assignment problem: $\min_{\mathbf{p} \in \Omega} \mathbf{m}_1^\top \mathbf{p}$. $\boldsymbol{\theta}$ can be recovered by solving the following low dimensional quadratic optimization problem:

$$\min \boldsymbol{\theta}^\top (\mathbf{C} + \mathbf{D})\boldsymbol{\theta} + \mathbf{m}_0^\top \boldsymbol{\theta} \quad (26)$$

$$\text{s.t. } \underline{\boldsymbol{\theta}} \leq \boldsymbol{\theta} \leq \bar{\boldsymbol{\theta}} \quad (27)$$

Solvers such as the matlab function *quadprog* can be used for this problem. The following result indicates that this is a convex problem.

Proposition 2: We have $\mathbf{C} + \mathbf{D} \succeq 0$.

Proof For any $\mathbf{p} \in \Omega$, we have $\text{mat}(\mathbf{B}\mathbf{p}) = \mathbf{J}_2^\top ((\mathbf{P}\mathbf{1}_{n_y}) \otimes \mathbf{I}_{n_\theta}) = \sum_i \mathbf{J}_i^\top \mathbf{J}_i (\mathbf{P}\mathbf{1}_{n_y})_i \succeq 0$. Since $\mathbf{p}_0 \in \Omega$, thus we have $\text{mat}(\mathbf{B}\mathbf{p}_0) = \text{mat}(\mathbf{K}\mathbf{B}_2\mathbf{p}_0) + \mathbf{C} = \mathbf{D} + \mathbf{C} \succeq 0$.

F. Upper bound of the objective function

By plugging the $\mathbf{p}, \boldsymbol{\theta}$ solutions yielded during the computation of the lower bound into $E(\mathbf{p}, \boldsymbol{\theta})$, we can get an upper bound. Nevertheless, the $\boldsymbol{\theta}$ solution may deviate significantly from the optimal $\boldsymbol{\theta}$ especially during the early iterations of the BnB algorithm, causing the computed upper bound to be poor. To address this issue, based on a result of [14], the objective function $E(\mathbf{P}, \boldsymbol{\theta})$ can be rewritten as a function of \mathbf{P} by eliminating $\boldsymbol{\theta}$:

$$E(\mathbf{p}) = -\mathbf{p}^\top \mathbf{A}^\top [\text{mat}(\mathbf{K}\mathbf{B}_2\mathbf{p}) + \mathbf{C}]^{-1} \mathbf{A}\mathbf{p} + \boldsymbol{\rho}^\top \mathbf{p} \quad (28)$$

Therefore, we can plug the computed \mathbf{p} into this function to get the value of E , which is used as an upper bound.

V. CASE TWO: 3D RIGID TRANSFORMATION

A 3D affine transformation has many parameters, causing our algorithm to be inefficient. Therefore, for the 3D case, we instead focus on rigid transformation.

Using the angle-axis representation, each 3D rotation can be represented as a 3D vector \mathbf{r} , with axis $\mathbf{r}/\|\mathbf{r}\|$ and angle $\|\mathbf{r}\|$. The corresponding 3×3 rotation matrix $\mathbf{R} \in \mathbb{S}\mathbb{O}_3$ for \mathbf{r} can be obtained using matrix exponential map as [11]

$$\mathbf{R} = \mathbf{I}_3 + \frac{[\mathbf{r}]_\times \sin \|\mathbf{r}\|}{\|\mathbf{r}\|} + \frac{[\mathbf{r}]_\times^2 (1 - \cos \|\mathbf{r}\|)}{\|\mathbf{r}\|^2} \quad (29)$$

where $[\cdot]_\times$ denotes the skew-symmetric matrix representation:

$$[\mathbf{r}]_\times = \begin{bmatrix} 0 & -r_3 & r_2 \\ r_3 & 0 & -r_1 \\ -r_2 & r_1 & 0 \end{bmatrix} \quad (30)$$

where r_i is the i -th element of \mathbf{r} .

Following [15], we model point matching as a linear assignment-least square problem:

$$\begin{aligned} \min E(\mathbf{P}, \mathbf{R}, \mathbf{t}) &= \sum p_{ij} \|\mathbf{y}_j - \mathbf{R}\mathbf{x}_i - \mathbf{t}\|^2 \\ &= \mathbf{1}_{n_x}^\top \mathbf{P}\tilde{\mathbf{y}} + \tilde{\mathbf{x}}^\top \mathbf{P}\mathbf{1}_{n_y} + n_p \|\mathbf{t}\|^2 - 2\text{tr}(\mathbf{R}\mathbf{X}^\top \mathbf{P}\mathbf{Y}) \\ &\quad - 2\mathbf{t}^\top (\mathbf{Y}^\top \mathbf{P}^\top \mathbf{1}_{n_x} - \mathbf{R}\mathbf{X}^\top \mathbf{P}\mathbf{1}_{n_y}) \end{aligned} \quad (31)$$

$$\text{s.t. } \mathbf{P} \in \Omega, \mathbf{R} \in \mathbb{S}\mathbb{O}_3, \underline{\mathbf{r}}_0 \leq \mathbf{r} \leq \bar{\mathbf{r}}_0, \underline{\mathbf{t}}_0 \leq \mathbf{t} \leq \bar{\mathbf{t}}_0 \quad (32)$$

where the transformation is chosen as a rigid transformation with rotation matrix \mathbf{R} and translation \mathbf{t} . The matrix $\mathbf{X} \triangleq [\mathbf{x}_1, \dots, \mathbf{x}_{n_x}]^\top$ and $\mathbf{Y} \triangleq [\mathbf{y}_1, \dots, \mathbf{y}_{n_y}]^\top$. The vector $\tilde{\mathbf{x}} \triangleq [\|\mathbf{x}_1\|_2^2, \dots, \|\mathbf{x}_{n_x}\|_2^2]^\top$. The constant vectors $\underline{\mathbf{r}}_0, \bar{\mathbf{r}}_0$ (resp. $\underline{\mathbf{t}}_0, \bar{\mathbf{t}}_0$) define the bounds of \mathbf{r} (resp. \mathbf{t}).

In the following, first, we discuss the branching strategy (Sec. V-A). Then, we derive the lower bounding functions of bilinear and trilinear terms (Sec. V-B and V-C). These results are used to build the lower bounding function of the objective function (Sec. V-D). Then, we discuss the computation of upper bound and computation of the range of \mathbf{R} from the range of \mathbf{r} (Sec. V-E and V-F). Finally, we use point set normalization to satisfy a requirement when using the convex envelope of a trilinear monomial [19] (Sec. V-G).

A. Branching strategy

Based on the result in Sec. III-A, for the bilinear term $-2\mathbf{t}^\top \mathbf{Y}^\top \mathbf{P}^\top \mathbf{1}$, for its linear lower bound function to converge to it, we only need to branch the range of \mathbf{t} and let the range of $-2\mathbf{Y}^\top \mathbf{P}^\top \mathbf{1}$ fixed. Here, the range of $-2\mathbf{Y}^\top \mathbf{P}^\top \mathbf{1}$ is computed as $\min_{\mathbf{p} \in \Omega} (-2\mathbf{Y}^\top \mathbf{P}^\top \mathbf{1})_i \leq (-2\mathbf{Y}^\top \mathbf{P}^\top \mathbf{1})_i \leq \max_{\mathbf{p} \in \Omega} (-2\mathbf{Y}^\top \mathbf{P}^\top \mathbf{1})_i$ via solving linear assignment problems.

Likewise, for the bilinear term $-2\text{tr}(\mathbf{R}\mathbf{X}^\top \mathbf{P}\mathbf{Y})$, we only need to branch the range of \mathbf{r} (since the range of \mathbf{r} determines the range of \mathbf{R}) and let the range of $-2\mathbf{X}^\top \mathbf{P}\mathbf{Y}$ fixed. Here, the range of $-2\mathbf{X}^\top \mathbf{P}\mathbf{Y}$ is computed as $\min_{\mathbf{p} \in \Omega} (-2\mathbf{X}^\top \mathbf{P}\mathbf{Y})_{ij} \leq (-2\mathbf{X}^\top \mathbf{P}\mathbf{Y})_{ij} \leq \max_{\mathbf{p} \in \Omega} (-2\mathbf{X}^\top \mathbf{P}\mathbf{Y})_{ij}$ via solving linear assignment problems.

In a similar vein, based on the result in Sec. III-B, for the trilinear term $2\mathbf{t}^\top \mathbf{R}\mathbf{X}^\top \mathbf{P}\mathbf{1}$, for its linear lower bounding function to converge to it, we only need to branch the ranges of \mathbf{r} and \mathbf{t} and let the range of $2\mathbf{X}^\top \mathbf{P}\mathbf{1}$ fixed. Here, the range of $2\mathbf{X}^\top \mathbf{P}\mathbf{1}$ is computed as $\min_{\mathbf{p} \in \Omega} (2\mathbf{X}^\top \mathbf{P}\mathbf{1})_j \leq (2\mathbf{X}^\top \mathbf{P}\mathbf{1})_j \leq \max_{\mathbf{p} \in \Omega} (2\mathbf{X}^\top \mathbf{P}\mathbf{1})_j$ via solving linear assignment problems.

To sum up, in our BnB algorithm, we only need to branch over \mathbf{r} and \mathbf{t} . Thus, the dimension of the branching space of our BnB algorithm is low and our algorithm can converge quickly.

B. Lower bounding function of the bilinear terms

Based on the result in Sec. III-A, we can get the lower bounding function of $-2\text{tr}(\mathbf{R}\mathbf{X}^\top \mathbf{P}\mathbf{Y}) = \sum_{ij} R_{ij}(-2\mathbf{Y}^\top \mathbf{P}^\top \mathbf{X})_{ij}$ within ranges $\underline{R}_{ij} \leq R_{ij} \leq \bar{R}_{ij}$ and $\min_{\mathbf{p} \in \Omega} (-2\mathbf{Y}^\top \mathbf{P}^\top \mathbf{X})_{ij} \leq (-2\mathbf{Y}^\top \mathbf{P}^\top \mathbf{X})_{ij} \leq \max_{\mathbf{p} \in \Omega} (-2\mathbf{Y}^\top \mathbf{P}^\top \mathbf{X})_{ij}$ by first computing the lower bounding functions of individual terms $R_{ij}(-2\mathbf{Y}^\top \mathbf{P}^\top \mathbf{X})_{ij}$:

$$C_{ij}^0 R_{ij} + C_{ij}^1 (-2\mathbf{Y}^\top \mathbf{P}^\top \mathbf{X})_{ij} + C_{ij}^2 \leq R_{ij} (-2\mathbf{Y}^\top \mathbf{P}^\top \mathbf{X})_{ij} \quad (33)$$

where the constant matrices \mathbf{C}^k are computed based on the ranges of R_{ij} and $(-2\mathbf{Y}^\top \mathbf{P}^\top \mathbf{X})_{ij}$. Now, we can get the lower bounding function of $-2\text{tr}(\mathbf{R}\mathbf{X}^\top \mathbf{P}\mathbf{Y})$ by summing the result in (33) over i and j :

$$\text{tr}(\mathbf{C}^0 \mathbf{R}^\top) - 2\text{tr}(\mathbf{C}^1 \mathbf{X}^\top \mathbf{P}\mathbf{Y}) + \mathbf{1}_3^\top \mathbf{C}^2 \mathbf{1}_3 \leq -2\text{tr}(\mathbf{R}\mathbf{X}^\top \mathbf{P}\mathbf{Y}) \quad (34)$$

Similarly, we can get the lower bounding function of $-2\mathbf{t}^\top \mathbf{Y}^\top \mathbf{P}^\top \mathbf{1} = \sum_i t_i (-2\mathbf{Y}^\top \mathbf{P}^\top \mathbf{1})_i$ within ranges $\underline{t}_i \leq t_i \leq \bar{t}_i$ and $\min_{\mathbf{p} \in \Omega} (-2\mathbf{Y}^\top \mathbf{P}^\top \mathbf{1})_i \leq (-2\mathbf{Y}^\top \mathbf{P}^\top \mathbf{1})_i \leq \max_{\mathbf{p} \in \Omega} (-2\mathbf{Y}^\top \mathbf{P}^\top \mathbf{1})_i$ by first computing the lower bounding functions of individual terms $t_i (-2\mathbf{Y}^\top \mathbf{P}^\top \mathbf{1})_i$:

$$d_i^0 t_i + d_i^1 (-2\mathbf{Y}^\top \mathbf{P}^\top \mathbf{1})_i + d_i^2 \leq t_i (-2\mathbf{Y}^\top \mathbf{P}^\top \mathbf{1})_i \quad (35)$$

where the constant vectors \mathbf{d}^j are computed based on the ranges of t_i and $(-2\mathbf{Y}^\top \mathbf{P}^\top \mathbf{1})_i$. Now, we can get the lower bounding function of $-2\mathbf{t}^\top \mathbf{Y}^\top \mathbf{P}^\top \mathbf{1}$ by summing the result in (35) over i :

$$\mathbf{t}^\top \mathbf{d}^0 - 2\mathbf{1}^\top \mathbf{P}\mathbf{Y} \mathbf{d}^1 + \mathbf{1}_3^\top \mathbf{d}^2 \leq -2\mathbf{t}^\top \mathbf{Y}^\top \mathbf{P}^\top \mathbf{1} \quad (36)$$

C. Lower bounding function of the trilinear term

Based on the result in Sec. III-B, we can get the lower bounding function of $2\mathbf{t}^\top \mathbf{R}\mathbf{X}^\top \mathbf{P}\mathbf{1} = \sum_{ij} t_i R_{ij} (2\mathbf{X}^\top \mathbf{P}\mathbf{1})_j$ within ranges $\underline{R}_{ij} \leq R_{ij} \leq \bar{R}_{ij}$, $\underline{t}_i \leq t_i \leq \bar{t}_i$ and $\min_{\mathbf{p} \in \Omega} (2\mathbf{X}^\top \mathbf{P}\mathbf{1})_j \leq (2\mathbf{X}^\top \mathbf{P}\mathbf{1})_j \leq \max_{\mathbf{p} \in \Omega} (2\mathbf{X}^\top \mathbf{P}\mathbf{1})_j$ by first computing the lower bounding functions of individual terms $t_i R_{ij} (2\mathbf{X}^\top \mathbf{P}\mathbf{1})_j$:

$$t_i F_{ij}^0 + F_{ij}^1 R_{ij} + F_{ij}^2 (2\mathbf{X}^\top \mathbf{P}\mathbf{1})_j + F_{ij}^3 \leq t_i R_{ij} (2\mathbf{X}^\top \mathbf{P}\mathbf{1})_j \quad (37)$$

where the constant matrices \mathbf{F}^k are computed based on the ranges of R_{ij} , t_i and $(2\mathbf{X}^\top \mathbf{P}\mathbf{1})_j$. Now, we can get the lower bounding function of $2\mathbf{t}^\top \mathbf{R}\mathbf{X}^\top \mathbf{P}\mathbf{1}$ by summing the result in (37) over i and j :

$$\begin{aligned} \mathbf{t}^\top \mathbf{F}^0 \mathbf{1}_3 + \text{tr}((\mathbf{F}^1)^\top \mathbf{R}) + 2\mathbf{1}_3^\top \mathbf{F}^2 \mathbf{X}^\top \mathbf{P}\mathbf{1}_{n_y} + \mathbf{1}_3^\top \mathbf{F}^3 \mathbf{1}_3 \\ \leq 2\mathbf{t}^\top \mathbf{R}\mathbf{X}^\top \mathbf{P}\mathbf{1}_{n_y} \end{aligned} \quad (38)$$

D. Lower bound of the objective function

Combining the results in Sec. V-B and V-C, we get lower bounding problem of the original problem (31), (32) as

$$\begin{aligned} \min E_l(\mathbf{P}, \mathbf{R}, \mathbf{t}) \triangleq n_p \|\mathbf{t}\|^2 + \mathbf{g}_0^\top \mathbf{t} + \text{tr}(\mathbf{G}_1 \mathbf{P}) \\ + \text{tr}(\mathbf{G}_2 \mathbf{R}) + g_3 \end{aligned} \quad (39)$$

$$\text{s.t. } \mathbf{P} \in \Omega, \underline{\mathbf{R}} \leq \mathbf{R} \leq \bar{\mathbf{R}}, \mathbf{R} \in \mathbb{S}\mathbb{O}_3, \underline{\mathbf{t}} \leq \mathbf{t} \leq \bar{\mathbf{t}} \quad (40)$$

where the vector $\mathbf{g}_0 \triangleq \mathbf{d}^0 + \mathbf{F}^0 \mathbf{1}_3$, the matrices $\mathbf{G}_1 \triangleq -2\mathbf{Y}\mathbf{C}^1 \mathbf{X}^\top - 2\mathbf{Y}\mathbf{d}^1 \mathbf{1}_{n_x}^\top + 2\mathbf{1}_{n_y} \mathbf{1}_3^\top \mathbf{F}^2 \mathbf{X}^\top + \tilde{\mathbf{y}} \mathbf{1}_{n_x}^\top + \mathbf{1}_{n_y} \tilde{\mathbf{x}}^\top$, $\mathbf{G}_2 \triangleq (\mathbf{C}^0)^\top + (\mathbf{F}^1)^\top$ and the scalar $g_3 \triangleq \mathbf{1}_3^\top \mathbf{C}^2 \mathbf{1}_3 + \mathbf{1}_3^\top \mathbf{d}^2 + \mathbf{1}_3^\top \mathbf{F}^3 \mathbf{1}_3$.

It is obvious that this problem can be decomposed into separate optimizations over \mathbf{P} , \mathbf{R} and \mathbf{t} . \mathbf{P} can be recovered by solving the following linear assignment problem: $\min_{\mathbf{p} \in \Omega} \text{tr}(\mathbf{G}_1 \mathbf{P})$.

\mathbf{R} can be recovered by solving the following optimization problem:

$$\begin{aligned} \min \text{tr}(\mathbf{G}_2 \mathbf{R}) \\ \text{s.t. } \underline{\mathbf{R}} \leq \mathbf{R} \leq \bar{\mathbf{R}}, \mathbf{R} \in \mathbb{S}\mathbb{O}_3 \end{aligned} \quad (41)$$

This problem is still difficult. We further relax this problem by dropping the constraint $\mathbf{R} \in \mathbb{S}\mathbb{O}_3$. Then the remaining problem is a low dimensional linear program which can be solved by solvers such as the Matlab function *linprog*.

\mathbf{t} can be recovered by solving the following low dimensional convex quadratic problem:

$$\min n_p \|\mathbf{t}\|^2 + \mathbf{g}_0^\top \mathbf{t} \quad (42)$$

$$\text{s.t. } \underline{\mathbf{t}} \leq \mathbf{t} \leq \bar{\mathbf{t}} \quad (43)$$

Solvers such as the matlab function *quadprog* can be used for this problem.

E. Upper bound of the objective function

Since the matrix \mathbf{R} yielded in Sec. V-D is not a valid rotation matrix, we can not directly plug the computed \mathbf{P} , \mathbf{R} , \mathbf{t} into $E(\mathbf{P}, \mathbf{R}, \mathbf{t})$ to get an upper bound. Instead, based on

a result of [15], the objective function $E(\mathbf{P}, \mathbf{R}, \mathbf{t})$ can be rewritten as a function of \mathbf{P} by eliminating \mathbf{t} and \mathbf{R} :

$$E(\mathbf{P}) = \mathbf{1}^\top \mathbf{P} \tilde{\mathbf{y}} + \tilde{\mathbf{x}}^\top \mathbf{P} \mathbf{1} - \frac{1}{n_p} (\|\mathbf{Y}^\top \mathbf{P}^\top \mathbf{1}\|^2 + \|\mathbf{X}^\top \mathbf{P} \mathbf{1}\|^2) - 2 \min_{\mathbf{R} \in \text{SO}_3} \left\{ \text{tr}(\mathbf{R}(\mathbf{X}^\top \mathbf{P} \mathbf{Y} - \frac{1}{n_p} \mathbf{X}^\top \mathbf{P} \mathbf{1} \mathbf{1}^\top \mathbf{P} \mathbf{Y})) \right\} \quad (44)$$

Therefore, we can plug the computed \mathbf{P} into this function to get the value of E , which is used as an upper bound. Here the optimal \mathbf{R} is computed by first computing the singular value decomposition of $(\mathbf{X}^\top \mathbf{P} \mathbf{Y} - \frac{1}{n_p} \mathbf{X}^\top \mathbf{P} \mathbf{1} \mathbf{1}^\top \mathbf{P} \mathbf{Y})^\top$ as $\mathbf{U} \mathbf{S} \mathbf{V}^\top$, where \mathbf{S} is a diagonal matrix and the columns of \mathbf{U} and \mathbf{V} are orthogonal unity vectors. Then the optimal \mathbf{R} is $\mathbf{R}^* = \text{Udiag}([1, \dots, 1, \det(\mathbf{U} \mathbf{V}^\top)]) \mathbf{V}^\top$ [20].

F. The range of \mathbf{R}

Given a range $[\mathbf{r}, \bar{\mathbf{r}}]$ of \mathbf{r} , based on (29), we can compute the range of \mathbf{R} as $\min\{R_{ij} | \mathbf{r} \leq \mathbf{r} \leq \bar{\mathbf{r}}\} \leq R_{ij} \leq \max\{R_{ij} | \mathbf{r} \leq \mathbf{r} \leq \bar{\mathbf{r}}\}$ via solvers such as the Matlab function *fmincon*. But this optimization can be cumbersome, especially when it is repeatedly executed as a subroutine of the BnB algorithm. To address this issue, we utilize the idea of precomputation to speed up the process: Before executing our BnB algorithm, we build a regular grid (whose width is chosen as 150 in this work) over the initial cube $[\underline{\mathbf{r}}_0, \bar{\mathbf{r}}_0]$. We then compute the corresponding R_{ij} values for all the grid points and store them. During the execution of our BnB algorithm, given a range $[\mathbf{r}, \bar{\mathbf{r}}]$, we first find the grid points falling within this range. We then compute the minimum and maximum of the precomputed R_{ij} values of these points, which are used to approximate $\min\{R_{ij} | \mathbf{r} \leq \mathbf{r} \leq \bar{\mathbf{r}}\}$ and $\max\{R_{ij} | \mathbf{r} \leq \mathbf{r} \leq \bar{\mathbf{r}}\}$.

G. Point set normalization

[19] only presents the convex envelope of a trilinear monomial under the condition that at least one variable that makes up the monomial has a range containing the origin, whereas for the trilinear term $2\mathbf{t}^\top \mathbf{R} \mathbf{X}^\top \mathbf{P} \mathbf{1}$, such a condition may be violated. To address this issue, note that the ranges of t_i and R_{ij} change during the BnB procedure, whereas the range of $(\mathbf{X}^\top \mathbf{P} \mathbf{1})_j$ remains fixed. Therefore, we seek to ensure that the range of $(\mathbf{X}^\top \mathbf{P} \mathbf{1})_j$ contains the origin. This can be accomplished as follows: We translate \mathcal{X} such that its center locates at the origin: $\frac{1}{n_p} \mathbf{X}^\top \mathbf{1} = 0$. Then the mean of the sum of the coordinates of any n_p number of points in \mathcal{X} also equals zero: $\frac{1}{|\Theta|} \sum_{\mathbf{P} \in \Theta} \mathbf{X}^\top \mathbf{P} \mathbf{1} = 0$, where the set $\Theta \triangleq \Omega \cap \{\mathbf{P} | p_{ij} \in \{0, 1\}\}$. Therefore, the range of $(\mathbf{X}^\top \mathbf{P} \mathbf{1})_j$ will contain the origin.

VI. BNB ALGORITHM

Based on the above preparation, we now can use the BnB algorithm to optimize E , which is summarized in Algo. 1, where the initial hypercube M is set as $[\underline{\boldsymbol{\theta}}_0, \bar{\boldsymbol{\theta}}_0]$ for the case that transformation is linear w.r.t. its parameters or $\{(\mathbf{r}, \mathbf{t}) | \mathbf{r} \in [\underline{\mathbf{r}}_0, \bar{\mathbf{r}}_0], \mathbf{t} \in [\underline{\mathbf{t}}_0, \bar{\mathbf{t}}_0]\}$ for the case that transformation is 3D rigid. Here note that for the case that transformation is linear w.r.t. its parameters, the vector form of the point correspondence variable is more convenient. Thus, the notations \mathbf{P} ,

\mathbf{P}^k and \mathbf{P}^{k-1} should to be replaced by \mathbf{p} , \mathbf{p}^k and \mathbf{p}^{k-1} , respectively.

Since the optimal transformation parameters depends on the relative size and position of two point sets, in this work, we rescale point sets \mathcal{X} and \mathcal{Y} to be unit sized and translate them to be centered at the origin before alignment. We set the bounds $\underline{\boldsymbol{\theta}}_0 = -3\mathbf{1}_{n_\theta}$, $\bar{\boldsymbol{\theta}}_0 = 3\mathbf{1}_{n_\theta}$, $\underline{\mathbf{r}}_0 = -\pi\mathbf{1}_3$, $\bar{\mathbf{r}}_0 = \pi\mathbf{1}_3$, $\underline{\mathbf{t}}_0 = -3\mathbf{1}_3$, $\bar{\mathbf{t}}_0 = 3\mathbf{1}_3$. The tolerance error ϵ should be set taking into account the cardinalities of two point sets. We empirically set it as $\epsilon = \min(n_x, n_y)\epsilon_0$, where ϵ_0 is a predefined positive scalar.

Algorithm 1: A BnB algorithm for minimizing E

- 1 **Initialization**
 - 2 Set tolerance error $\epsilon > 0$ and initial hypercube M . Let $\mathcal{M}_1 = \mathcal{N}_1 = \{M\}$ where \mathcal{M}_k and \mathcal{N}_k denote the collection of all hypercubes and the collection of active hypercubes at iteration k , respectively.
 - 3 **for** $k = 1, 2, \dots$ **do**
 - 4 For each hypercube $M \in \mathcal{N}_k$, minimize the lower bounding function E_l to obtain the optimal point correspondence solution $\mathbf{P}(M)$ and the optimal value $\beta(M)$. $\beta(M)$ is a lower bound for M .
 - 5 Let \mathbf{P}^k be the best among all feasible solutions so far encountered: \mathbf{P}^{k-1} and all $\mathbf{P}(M)$ for $M \in \mathcal{N}_k$. Delete all $M \in \mathcal{M}_k$ such that $\beta(M) \geq E(\mathbf{P}^k) - \epsilon$. Let \mathcal{R}_k be the remaining collection of hypercubes.
 - 6 If $\mathcal{R}_k = \emptyset$, terminate: \mathbf{P}^k is the global ϵ -minimum solution.
 - 7 Select the hypercube M yielding the lowest lower bound and divide it into two sub-hypercubes M_1, M_2 by bisecting the longest edge.
 - 8 Let $\mathcal{N}_{k+1} = \{M_1, M_2\}$ and $\mathcal{M}_{k+1} = (\mathcal{R}_k \setminus M) \cup \mathcal{N}_{k+1}$.
 - 9 **end**
-

VII. EXPERIMENTS

We implement our method (denoted by RPM-HTB) under Matlab 2019b and compare it with other methods on a PC with 3.5 GHz CPU. For the competing methods which only output point correspondence, the generated point correspondence is used to compute the best affine transformation between two point sets. We define error as the root-mean-square difference between the coordinates of transformed ground truth model inliers and those of their corresponding scene inliers.

A. Case one: transformation is linear w.r.t. its parameters

We compare RPM-HTB with RPM-CAV [15] and Go-ICP [11]. Both of them are based on global optimization, can handle partial overlapping point sets and allow arbitrary rotation and translation between two point sets.

2D similarity and affine transformations are respectively considered for RPM-HTB. For the former, we have $\mathbf{J}(\mathbf{x}_i) = \begin{bmatrix} x_i^1 & -x_i^2 & 1 & 0 \\ x_i^2 & x_i^1 & 0 & 1 \end{bmatrix}$ and $\mathbf{B}_2 = \mathbf{B}([1, 3, 4], :)$. For the latter,

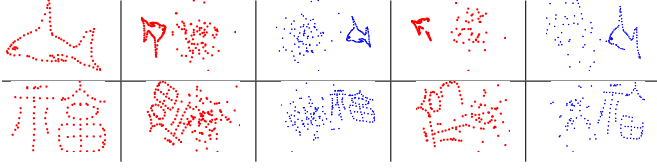


Fig. 1. Left column: the prototype shapes. For the remaining columns: examples of model and scene point sets in the outlier (columns 2, 3) and occlusion + outlier (columns 4, 5) tests.

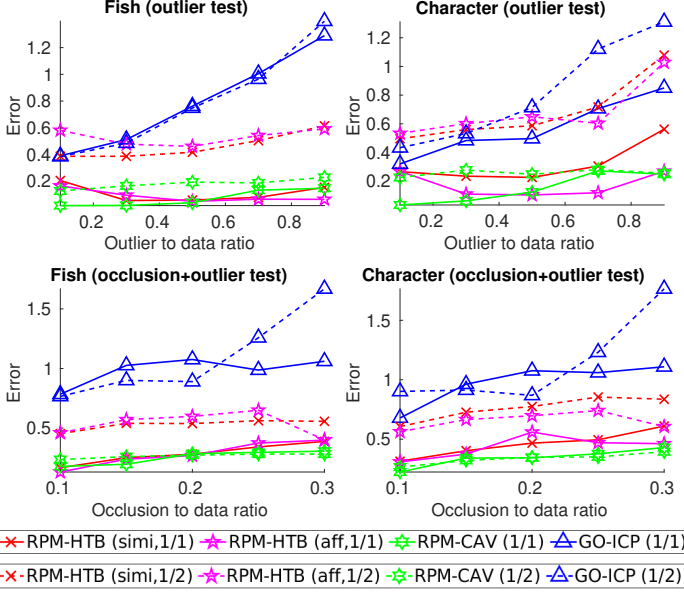


Fig. 2. Average matching errors by RPM-HTB, RPM-CAV and Go-ICP with different n_p values (chosen from 1/2 to 1/1 the ground truth value) over 100 random trials for the 2D outlier and occlusion+outlier tests.

we have $\mathbf{J}(\mathbf{x}_i) = \begin{bmatrix} x_i^1 & x_i^2 & 0 & 0 & 1 & 0 \\ 0 & 0 & x_i^1 & x_i^2 & 0 & 1 \end{bmatrix}$ and $\mathbf{B}_2 = \mathbf{B}([1, 2, 5, 8, 11], :)$. For RPM-HTB, we set $\epsilon_0 = 8$.

Synthetic data is easy to obtain and can be used to test specific aspects of an algorithm. Following [14], two categories of tests are conducted: 1) **Outlier test** and 2) **Occlusion + Outlier test**. Different from [14], disturbances of random rotation and scaling within range $[0.5, 1.5]$ are also added when generating the point sets. Fig. 1 illustrates these tests and Fig. 2 illustrates the matching errors by different methods. RPM-HTB and RPM-CAV with n_p value close to the ground truth performs the best. In terms of different choices of transformations, our method using affine transformation performs slightly better. In terms of different choices of n_p , RPM-HTB with n_p value close to the ground truth performs better. Examples of alignment results by different methods are illustrated in Fig. 3.

The average running times (in seconds) are: 10.08 or 757.81 for RPM-HTB using similarity or affine transformation, 2.24 for RPM-CAV and 11.30 for Go-ICP. This demonstrates good efficiency of our method using similarity transformation. Our method using affine transformation is an order of magnitude slower than when using similarity transformation. This is because affine transformation has more number of parameters.

1) *2D point sets extracted from images*: Point sets extracted from images are a realistic setting for testing algorithms. We

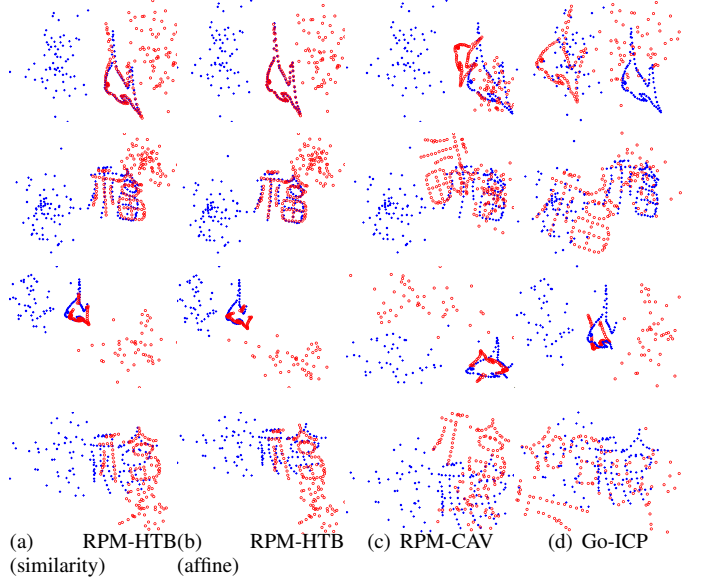


Fig. 3. Examples of alignment results by RPM-HTB, RPM-CAV and Go-ICP with n_p value chosen as the ground truth for the 2D outlier (top 2 rows) and occlusion+outlier (bottom 2 rows) tests.

test different alignment methods on 2D point sets extracted via the Canny edge detector from several images coming from the Caltech-256 [10] and VOC2007 [7] datasets, as illustrated in Fig. 4. To test a method’s ability at handling rotation, model point sets are rotated 180° before being matched to scene point sets.

The alignment results by different methods are presented in Fig. 4. RPM-HTB using similarity transformation performs the best. In comparison, RPM-CAV does not fit the wheels tightly and aligns some eiffel towers tiltedly. RPM-HTB using affine transformation does not perform well. This is because affine transformation contains too much transformation freedom, thus is less robust against heavy clutters.

B. Case two: 3D rigid transformation

Since RPM-CAV is inefficient for the 3D case, it is not compared. Instead, we compare with FRS [22], which is based on global optimization and allows arbitrary rigid transformation between two point sets. Finally, we compare with a heuristic variant of RPM-HTB where $\epsilon_0 = 0$ and the maximum branching depth is set as 10 instead of infinity.

Analogous to the experimental setup in Sec. VII-A, we conduct two categories of tests: 1) **Outlier test** and 2) **Occlusion + Outlier test**. Fig. 5 illustrates these tests and Fig. 6 illustrates the matching errors by different methods. For the outlier test, RPM-HTB and its variant with n_p value chosen as the ground truth performs overall better than other methods. For the occlusion + outlier test, RPM-HTB and its variant perform similarly as Go-ICP until occlusion becomes severe. This indicates that our method is suitable for the problems where occlusion is not severe. In terms of different choices of n_p , RPM-HTB and its variant with n_p value close to the ground truth perform much better. Finally, one can observe that for the outlier test, the error by RPM-HTB actually

decreases with the increase of outliers. This can be easily remedied by setting ϵ lower than is determined by the formula $\epsilon = \min(n_x, n_y)\epsilon_0$ when outliers are few. Alternative better formulas of ϵ will be explored in the future. Examples of alignment results by different methods are illustrated in Fig. 7.

The average running time (in seconds) are: 72.45 for RPM-HTB, 22.33 for the RPM-HTB variant, 33.04 for Go-ICP and 198.62 for FRS. The efficiency by our method is close to that of Go-ICP and much better than that of FRS.

VIII. CONCLUSION

We proposed a BnB based alignment algorithm which can handle partially overlapping point sets and is invariant to the corresponding transformation. For our algorithm, the lower bound is efficiently obtained via linear assignment and low dimensional convex quadratic programming. The branching space has a dimension equal to the number of transformation parameters. This enables our method to converge quickly. Experimental results demonstrated favorable robustness and efficiency of the proposed method in comparison to the state-of-the-art approaches.

ACKNOWLEDGMENTS

This work was supported by National Natural Science Foundation of China under Grant 61773002.

REFERENCES

- [1] J.-C. Bazin, Y. Seo, and M. Pollefeys. Globally optimal consensus set maximization through rotation search. In *Asian Conference on Computer Vision*, 2012.
- [2] Paul J. Besl and Neil D. McKay. A method for registration of 3-d shapes. *IEEE Trans. Pattern Analysis and Machine Intelligence*, 14(2):239–256, 1992.
- [3] Dylan Campbell and Lars Petersson. An adaptive data representation for robust point-set registration and merging. In *ICCV*, 2015.
- [4] Dylan Campbell and Lars Petersson. Gogma: Globally-optimal gaussian mixture alignment. In *The IEEE Conference on Computer Vision and Pattern Recognition*, June 2016.
- [5] Manmohan Chandraker and David Kriegman. Globally optimal bilinear programming for computer vision applications cvpr. 06 2008.
- [6] Haili Chui and Anand Rangarajan. A new point matching algorithm for non-rigid registration. *Computer Vision and Image Understanding*, 89(2-3):114–141, 2003.
- [7] M. Everingham, L. Van Gool, C. K. I. Williams, J. Winn, and A. Zisserman. The PASCAL Visual Object Classes Challenge 2007 (VOC2007) Results. <http://www.pascal-network.org/challenges/VOC/voc2007/workshop/index.html>.
- [8] Wei Gao and Russ Tedrake. Filterreg: Robust and efficient probabilistic point-set registration using gaussian filter and twist parameterization. In *CVPR*, 2019.
- [9] Lena Gorelick, Yuri Boykov, Olga Veksler, Ismail Ben Ayed, and Andrew Delong. Submodularization for quadratic pseudo-boolean optimization. In *CVPR*, 2014.
- [10] G. Griffin, A. Holub, and P. Perona. Caltech-256 object category dataset, 2007. technical report, California Inst. of Technology.
- [11] Yang J, Li H, Campbell D, and Jia Y. Go-icp: A globally optimal solution to 3d icp point-set registration. *IEEE Trans Pattern Anal Mach Intell.*, 38:2241–2254, 2016.
- [12] B. Jian and B. C. Vemuri. Robust point set registration using gaussian mixture models. *IEEE Trans. Pattern Analysis and Machine Intelligence*, 33(8):1633–1645, 2011.
- [13] Hongdong Li and Richard Hartley. The 3d-3d registration problem revisited. In *International Conference on Computer Vision*, 2007.
- [14] Wei Lian and Lei Zhang. Point matching in the presence of outliers in both point sets: A concave optimization approach. In *IEEE Conference on Computer Vision and Pattern Recognition*, pages 352–359, 2014.

- [15] Wei Lian and Lei Zhang. A concave optimization algorithm for matching partially overlapping point sets. *Pattern Recognition*, 103, 7 2020.
- [16] Wei Lian, Lei Zhang, and Ming-Hsuan Yang. An efficient globally optimal algorithm for asymmetric point matching. *IEEE Transactions on Pattern Analysis and Machine Intelligence*, 2016.
- [17] Yinlong Liu, Chen Wang, Zhijian Song, and Manning Wang. Efficient global point cloud registration by matching rotation invariant features through translation search. In *The European Conference on Computer Vision (ECCV)*.
- [18] C. Meyer and C. Floudas. *Trilinear monomials with positive or negative domains: facets of the convex and concave envelopes*, pages 327–352. 2003.
- [19] Clifford Meyer and Christodoulos Floudas. Trilinear monomials with mixed sign domains: Facets of the convex and concave envelopes. *Journal of Global Optimization*, 29:125–155, 06 2004.
- [20] Andriy Myronenko and Xubo Song. Point set registration: Coherent point drift. *IEEE Transactions on Pattern Analysis and Machine Intelligence*, 32(12):2262–2275, 2010.
- [21] Carl Olsson, Fredrik Kahl, and Magnus Oskarsson. Branch-and-bound methods for euclidean registration problems. *IEEE Transactions on Pattern Analysis and Machine Intelligence*, 31(5):783–794, 2009.
- [22] Álvaro Parra, Tat-Jun Chin, Anders Eriksson, Hongdong Li, and David Suter. Fast rotation search with stereographic projections for 3d registration. *IEEE Transactions on Pattern Analysis and Machine Intelligence*, 38(11):2227–2240, 2016.
- [23] J. Straub, T. Campbell, J. P. How, and J. W. Fisher. Efficient global point cloud alignment using bayesian nonparametric mixtures. In *Proc. IEEE Conf. Comput. Vis. Pattern Recog.*, pages 2403–2412, 2017.
- [24] Zhengyou Zhang. Iterative point matching for registration of free-form curves and surfaces. *International Journal of Computer Vision*, 13(2):119–152, 1994.

APPENDIX

Proposition 3: If $|\bar{x} - \underline{x}|$ or $|\bar{y} - \underline{y}|$ is sufficiently small, we will have $|xy - (xy)_l| \leq \epsilon$ for any $\epsilon > 0$.

Proof Since

$$(xy)_l \triangleq \frac{1}{2} \sum_i (xy)_{li} \\ = \frac{1}{2} (\underline{x} + \bar{x})y + \frac{1}{2} (\underline{y} + \bar{y})x - \frac{1}{2} (\underline{xy} + \bar{xy}) \quad (45)$$

therefore,

$$|xy - (xy)_l| = \\ \frac{1}{2} |(x - \underline{x})(y - \underline{y}) + (\bar{x} - x)(\bar{y} - y)| \\ \leq \frac{1}{2} |(x - \underline{x})(y - \underline{y})| + \frac{1}{2} |(\bar{x} - x)(\bar{y} - y)| \\ \leq |\bar{x} - \underline{x}| \cdot |\bar{y} - \underline{y}| \quad (46)$$

Therefore, if $|\bar{x} - \underline{x}|$ or $|\bar{y} - \underline{y}|$ is sufficiently small, we will have $|xy - (xy)_l| \leq \epsilon$ for any $\epsilon > 0$.

Proposition 4: If the ranges of any two variables that makes up xyz are sufficiently small, we will have $|xyz - (xyz)_l| \leq \epsilon$ for any $\epsilon > 0$.

Proof In the case $\underline{x} \leq 0, \underline{y} \geq 0, \underline{z} \leq 0, \bar{z} \geq 0$, we have the following inequalities (which has been presented in Sec. 3.2

of the main paper):

$$(xyz)_{11} \triangleq \underline{y}\bar{z}x + \bar{x}zy + \overline{xyz} - 2\overline{xyz} \leq xyz \quad (47)$$

$$(xyz)_{12} \triangleq \underline{y}\bar{z}x + \underline{x}\bar{z}y + \underline{x}\bar{y}z - \overline{xyz} - \underline{xyz} \leq xyz \quad (48)$$

$$(xyz)_{13} \triangleq \underline{y}\bar{z}x + \underline{x}zy + \underline{x}\bar{y}z - \overline{xyz} - \underline{xyz} \leq xyz \quad (49)$$

$$(xyz)_{14} \triangleq \underline{y}\bar{z}x + \bar{x}zy + \overline{xyz} - \overline{xyz} - \underline{xyz} \leq xyz \quad (50)$$

$$(xyz)_{15} \triangleq \underline{y}\bar{z}x + \bar{x}zy + \underline{x}\bar{y}z - \overline{xyz} - \underline{xyz} \leq xyz \quad (51)$$

$$(xyz)_{16} \triangleq \underline{y}\bar{z}x + \underline{x}\bar{z}y + \phi/(\bar{z} - \underline{z})z - \phi\underline{z}/(\bar{z} - \underline{z}) \\ - \underline{xyz} - \overline{xyz} + \overline{xyz} \leq xyz \quad (52)$$

where $\phi = \overline{xyz} - \overline{xyz} - \underline{xyz} + \underline{xyz}$.

For the first inequality (47), we have

$$\begin{aligned} & |xyz - (xyz)_{11}| \\ &= |xz(y - \bar{y}) + x\bar{y}(z - \bar{z}) + \bar{x}z(\bar{y} - y) + \overline{xy}(\bar{z} - z)| \\ &\leq |xz(y - \bar{y})| + |x\bar{y}(z - \bar{z})| + |\bar{x}z(\bar{y} - y)| + |\overline{xy}(\bar{z} - z)| \end{aligned} \quad (53)$$

Therefore, if $|\bar{y} - y|$ and $|\bar{z} - z|$ are sufficiently small, we will have $|xyz - (xyz)_{11}| \leq \epsilon$.

Similarly, we can prove

$$\begin{aligned} & |xyz - (xyz)_{11}| \\ &\leq |xz(y - \bar{y})| + |\bar{y}z(x - \bar{x})| + |\bar{y}\bar{z}(\bar{x} - x)| + |\bar{x}z(\bar{y} - y)| \end{aligned} \quad (54)$$

Therefore, if $|\bar{x} - x|$ and $|\bar{y} - y|$ are sufficiently small, we will have $|xyz - (xyz)_{11}| \leq \epsilon$.

Similarly, one can also prove

$$\begin{aligned} & |xyz - (xyz)_{11}| \\ &\leq |xy(z - \bar{z})| + |y\bar{z}(x - \bar{x})| + |\bar{y}\bar{z}(\bar{x} - x)| + |\overline{xy}(\bar{z} - z)| \end{aligned} \quad (55)$$

Therefore, if $|\bar{x} - x|$ and $|\bar{z} - z|$ are sufficiently small, we will have $|xyz - (xyz)_{11}| \leq \epsilon$.

To sum up, we will have $|xyz - (xyz)_{11}| \leq \epsilon$ if the ranges of any two variables that makes up xyz are sufficiently small. For other inequalities (48) to (52), we can prove similar results.

Based on the above results, therefore, for the average of the inequalities (47) to (52), we will have $|xyz - (xyz)_l| \leq \epsilon$ if the ranges of any two variables are sufficiently small.

For other cases of the bounds on x, y, z , we can prove similar results.

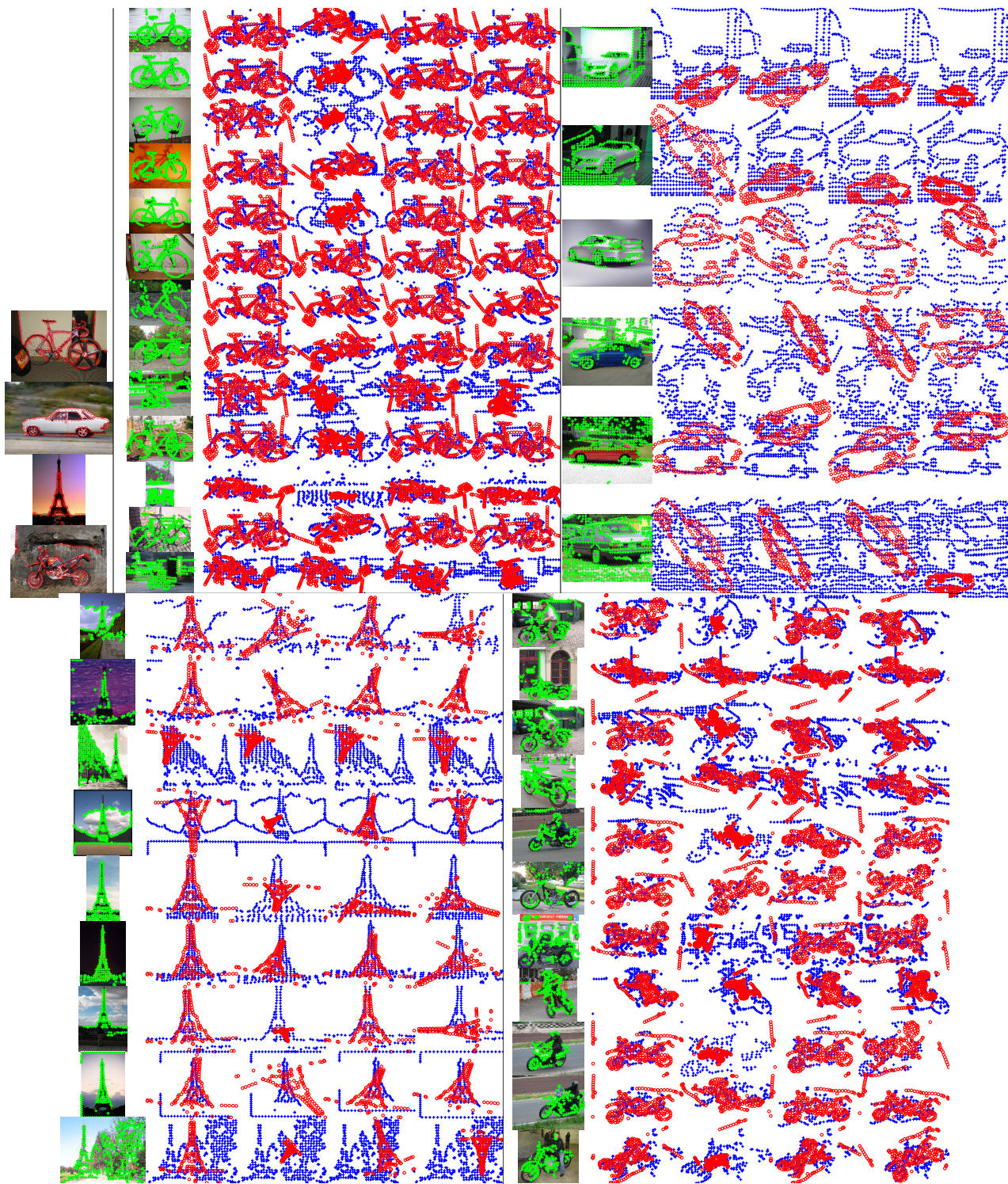


Fig. 4. Top left grid cell: model images with model point sets superimposed. The remaining cells: scene images with scene point sets superimposed, alignment results by RPM-HTB using similarity or affine transformations, RPM-CAV and Go-ICP. The n_p value for each method is chosen as 0.9 the minimum of the cardinalities of two point sets.

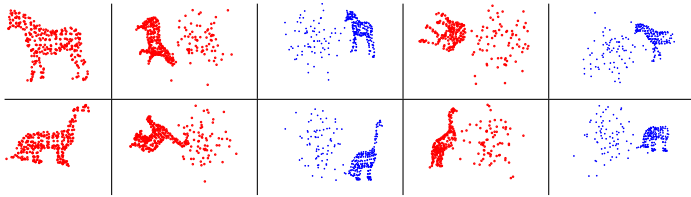


Fig. 5. Left column: the prototype shapes. For the remaining columns: examples of model and scene point sets in the outlier (columns 2, 3) and occlusion + outlier (columns 4, 5) tests.

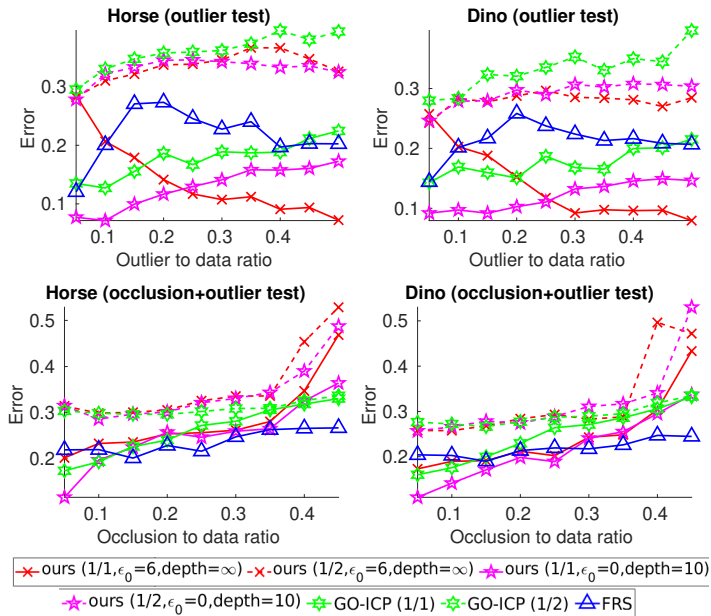


Fig. 6. Average matching errors by our method with different ϵ_0 values and maximum branching depths and Go-ICP under different n_p values (chosen from 1/2 to 1/1 the ground truth value) and FRS over 100 random trials for the 3D outlier and occlusion+outlier tests.

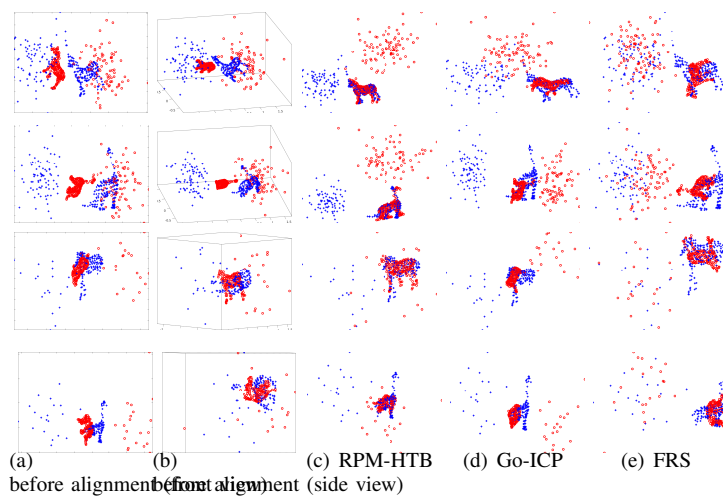


Fig. 7. Examples of alignment results by RPM-HTB and Go-ICP with n_p value chosen as the ground truth and FRS for the 3D outlier (top 2 rows) and occlusion+outlier (bottom 2 rows) tests.